Deep Learning-Based Roof Detection from UAV Dense Point Cloud for Solar Panels Mapping

Aleksandra Sekrecka , Damian Wierzbicki, Kinga Karwowska , Agniszka Myrcik

Department of Imagery Intelligence, Faculty of Civil Engineering and Geodesy, Military University of Technology,
00-908 Warsaw, Poland – (aleksandra.sekrecka;damian.wierzbicki;kinga Karwowska)@wat.edu.pl,
agnieszka.wojcik@student.wat.edu.pl

Keywords: remote sensing, point cloud processing, UAV, roof detection, semantic segmentation.

Abstract

Photovoltaic panels are becoming increasingly popular, and finding a suitable location for them quickly and automatically is a current and practical problem. In our experiment, we test whether a point cloud from dense multi-image matching can be useful for the automatic detection of the best locations for installing photovoltaic panels. We propose a methodology for processing and analyzing UAV point clouds, where the use of deep learning in combination with the CANUPO algorithm results in high roof recognition efficiency. Two classes were selected: roofs and non-roof objects. This made it possible to filter the detected roofs and remove erroneous objects. The resulting model detected buildings with an accuracy of approximately 80% and an effectiveness of 100% (there were no false detections). the following factors were taken into account in the insolation calculations: roof angles, roof slope exposure, changes in the angle of sunlight throughout the year, and atmospheric transmittance. The roof angles and exposure were determined using a Digital Surface Model (DSM) generated from multi-image UAV data. In our research, we took into account the average angle of incidence of sunlight throughout the year and at quarterly intervals. The use of DSM for roofs and the SVC algorithm combined with CANUPO made it possible to eliminate false detections and significantly increase the effectiveness of location detection. Research conducted for the entire year and quarters enabled the analysis of changes in roof insolation throughout the year, which is crucial when estimating the profitability of installing photovoltaic panels.

1. Introduction

The industrial revolution has contributed to environmental degradation and climate change, which is why new ways of generating electricity are being sought. One alternative to coal-fired power plants is solar energy, primarily because it is available everywhere on Earth. As a result, photovoltaic panels are becoming increasingly popular, and quickly and automatically finding a suitable location for them is a current and practical challenge.

As photogrammetric techniques have advanced, further research has been conducted on the use of photogrammetry to determine the location and efficiency of photovoltaic panels. Recent studies show that drone technology can yield promising results in high-resolution solar potential mapping (Ekawita et al., 2025). However, most studies focus on the use of photogrammetry to monitor existing solar farms. It is common to use LIDAR data and images captured from UAVs using RGB and thermal cameras to monitor individual solar panels on a photovoltaic farm (Cardoso et al., 2024; Henry et al., 2020; Huerta Herraiz et al., 2020).

The second important aspect is the use of photogrammetric data to identify potential locations for installing photovoltaic panels. High-resolution point clouds are a valuable source of data for roof segmentation. Meanwhile, photogrammetric products such as: Digital Terrain Models (DTMs), Digital Surface Models (DSMs) and orthoimages provide information for analyzing roof types and their parameters, such as area, slope angle, and roof orientation (Ekawita et al., 2025). (Martín-Jiménez et al., 2020) used LIDAR data and orthophotos to characterize the geometry of roofs in terms of slope and to calculate their photovoltaic potential. Their analysis took into account various locations and roof types.

In our research, we focus on using point clouds from a multi-image dataset collected by UAVs. A key step in this process is the detection of roofs, which are then subjected to further analysis. With the development of digital image processing techniques, various approaches to roof detection have emerged, which can be divided into two main groups: classical methods and machine learning-based methods. Classical methods rely on the analysis of photogrammetric products (such as DTM, DSM, and orthomosaics) and simple geometric rules. Roofs are detected on the difference model between the DSM and the DTM using threshold segmentation based on the height, shape, and slope of the surface (Guo et al. 2021; He et al. 2016; Nex and Remondino 2012). Rule-based methods primarily include region growing, the Hough transform, and Random Sample Consensus (RANSAC) (Tarsha-Kurdi et al., 2007). Research shows that a rule-based segmentation approach works well for roofs of low and medium complexity (Huerta Herraiz et al., 2020).

The rapid growth of machine learning has led to a significant increase in the popularity of methods based on these techniques (Yang et al., 2021) used an SC-BOVW model (sparse coding-enhanced bag of visual word) based on a trained discriminative dictionary, which encodes local geometric and spectral information within each supervoxel into a high-level semantic representation. This data is then fed into a Support Vector Machine (SVM) classifier to distinguish buildings from other objects. In contrast, the use of neural networks, such as PointNet++ or multiview CNNs (Shajahan et al., 2020; Zhang and Fan, 2022) with a self-attention mechanism, enables automatic segmentation and classification of roofs with high precision and accuracy. Recent studies have focused on the use of YOLO in roof monitoring and maintenance (Silva et al., 2025). In turn, (Kaya, 2026) applied the Mask R-CNN deep learning algorithm to automatically extract buildings from a UAV orthophoto map. Alternatively, (Singh et al., 2021) proposed using the multiscale CAractérisation de NUages de POints CANUPO classifier in combination with the RANSAC (random sample consensus) shape detection algorithm to monitor roof structures using LIDAR data.

Nevertheless, most publications focus on extracting roofs from RGB images or LIDAR point clouds. Far fewer publications discuss detecting roofs in point clouds derived from UAV data. (Kushwaha et al., 2019) combined the Cloth Simulation Filtering (CSF) and the CANUPO Classifier to detect roofs. (Błaszczak-Bąk et al., 2025) used UAV data for solar radiation analysis, but roof parameters were determined based on a 3D building model. Another approach (Bognár et al., 2021) uses the DSM directly as shading geometry, eliminating the need to generate 3D surface geometry and thereby simplifying the solar radiation analysis process.
Although UAV data has formed the basis of numerous studies for many years, the use of point clouds derived from multi-image registration of this data in planning the installation of photovoltaic panels on roofs remains an underdeveloped area. In our experiment, we investigate whether a point cloud derived from dense multi-image registration can be useful for the automatic detection of optimal locations for installing photovoltaic panels. We propose a methodology for processing and analyzing UAV point clouds, where the use of deep learning (Super-Voxel Clustering method -SVC) in combination with the CANUPO algorithm yields high roof recognition accuracy.

2. Data

The study was conducted in the village of Tuczępy in southern Poland. This area is characterized by detached residential buildings and farm structures. As it is a rural area, the landscape features vast agricultural fields, meadows, pastures, and forests. Two UAV flights (VTOL Wingtra) were conducted over the study area using a Sony RX1 RX2 42 Mpix camera with a 35 mm lens. Both flights took place in April at an altitude of 220 m, yielding images with a GSD of 4 cm. The lateral and longitudinal coverage of the images was 75%. The first flight collected data from the northern part of the village, and the second from the southern part. Data from the first flight were used as training data for roof detection. Data from flight 2 served as test data (Figure 1).

(a)

(b)

Figure 1. (a) Training and (b) test point cloud

3. Experiment

The experiment consisted of the following stages: creation of point clouds from multi-image registration; semantic segmentation of buildings using deep learning; roof/non-roof classification using the CANUPO classifier; and solar radiation analysis.

3.1 Generating a dense point cloud from a UAV

The photogrammetric blocks obtained from both flights were registered using GCPs (11 control points for Flight 1and 9 control points for Flight 2) (Figure 2).

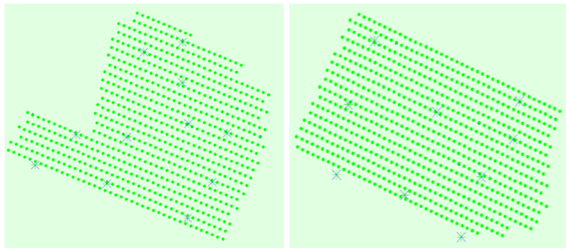

(a) (b)

Figure 2. Photogrammetric flight plan, including GCPs, for (a) the northern section (Flight 1) and (b) the southern section (Flight 2).

For each flight, control points were automatically generated to refine the adjustment. Table 1 presents the adjustment results for both photogrammetric blocks. The high number of tie points allowed for a highly accurate adjustment of the block, which in turn contributed to the high accuracy of the multi-image point cloud. The block adjustment error (σ_0) of adjustment in both cases was only 0.1 pixels, while the mean positional errors of the check points ($RMSE_X$, $RMSE_Y$, $RMSE_Z$) did not exceed 0.05 m.

		Lot 1	Lot 2
Number of 2D tie points		11105801	9886129
Number of 3D tie points		2628047	2517144
block adjustment error σ_0 [px]		0.1	0.1
Mean positional errors of control points	$RMSE_X$ [m]	0.02	0.05
	$RMSE_Y$ [m]	0.01	0.02
	$RMSE_Z$ [m]	0.02	0.03

Table 1. Accuracy of photogrammetric block adjustment for data from Flight 1 and Flight 2.

The Dense Matching technique, which involves determining depth values for each pixel, was used to generate a dense point cloud. For this purpose, the Semi-Global Matching (SGM) algorithm was used, which is one of the most popular methods of this type. The SGM algorithm optimizes the global energy function by applying dynamic programming along multiple paths, which allows for the generation of precise and consistent disparity maps (Ma et al., 2023). Ultimately, the point cloud for Flight 1 contained 146 million points with a density of 86 points/m³, while the point cloud for Flight 2 contained 186 million points with a density of 87 points/m³.

3.2 Segmentation and classification of roofs

In the next step, semantic segmentation was performed to detect roofs in the generated point cloud. The Super-Voxel Clustering (SVC) algorithm was used, which is based on Support Vector Machines (SVM). SVM is a set of supervised machine learning methods used for classification, segmentation, regression, and outlier detection. It works by finding an optimal hyperplane that maximizes the margin between different classes in a multidimensional feature space, often using the kernel trick to handle nonlinear data transformations (Cortes and Vapnik, 1995; Montesinos López et al., 2022). SVC makes no assumptions about the number or shape of clusters in the data, but uses the support vector domain description to identify the region in the data space where the input examples are concentrated. The goal of SVC is to partition a dataset into groups according to a certain criterion in order to organize the data into a more understandable form. In the SVC algorithm, data points are mapped from the data space to a multidimensional feature space using a kernel function. In the kernel feature space, the algorithm finds the smallest sphere S encompassing the data image using the support vector domain description algorithm. SVC classification follows the formula (1):

$$A_{ij} = \begin{cases} 1, if\ f(x) > 0\ i\ x \in S \\ 0,\ in\ other\ cases \end{cases} \quad (1)$$

where A_{ij} = a given set
x = elements of the set
S = a sphere in function space

SVC is a machine learning technique, so it was necessary to define a training dataset (buildings marked on the point cloud from Flight 1) and a test dataset (point cloud from flight 2). At this stage, the model produced many false positives (such as tree crowns). The result of the SVC segmentation is shown in Figure 3.

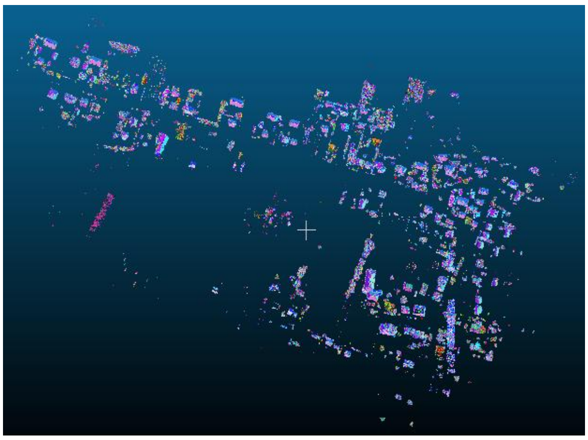

Figure 3. The resulting point cloud after semantic segmentation using the SVM method.

The CANUPO classifier is a machine learning method designed for the classification and segmentation of 3D point clouds. It works by analyzing the local geometric properties of points, such as roughness and morphological features, which enables the differentiation of various types of surfaces and objects. The algorithm is based on local measures of point dimensionality, and combining information from multiple scales leads to the creation of characteristic signatures that allow for the identification of individual object classes in the analyzed scene. These signatures are automatically determined based on training points, which aids in the process of optimizing the resolution between classes. Additionally, descriptors are created by integrating information from different scales, which increases recognition accuracy and enables the identification of diverse objects present in the scene (Ntuli et al., 2024).
Trained on samples of roofs and vegetation, CANUPO is able to distinguish between roof coverings and vegetation. Two classes were selected: roof and non-roof objects. This allowed for filtering the detected roofs and removing erroneous objects. Figure 4 presents the classifier's results: roofs are marked in blue, and other elements, such as vegetation, haystacks, and incomplete roof coverings, are marked in red. After filtering out the vegetation class, a resulting point cloud was obtained, showing only roofs.

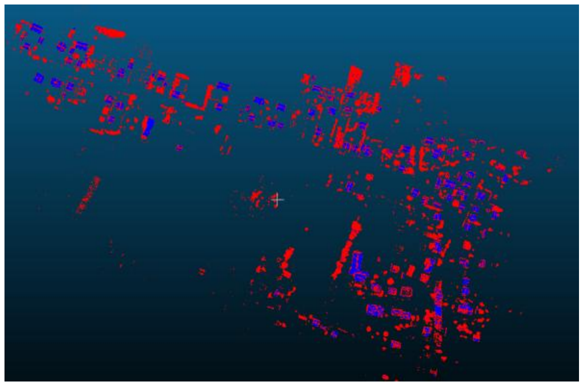

Figure 4. CANUPO classification results (red—vegetation, green—roofs).

3.3 Method of sun insolation analysis

The solar radiation analysis was performed using a hemispherical radiation algorithm based on the following equation ("How solar radiation is calculated—ArcGIS Pro | Documentation," n.d.):

$$Dir_{\theta,\alpha} = S_{Const} \cdot \beta^{m(\theta)} \cdot SunDur_{\theta,\alpha} \cdot SunGap_{\theta,\alpha} \cdot \cdot \cos(AngIn_{\theta,\alpha}) \quad (2)$$

where $Dir_{\theta,\alpha}$=direct insolation with a centroid at zenith angle (θ) and azimuth angle (α)
S_{Const} =the solar constant
$\beta^{m(\theta)}$ =the transmissivity of the atmosphere;
$SunDur_{\theta,\alpha}$ = the time duration represented by the sky sector
$SunGap_{\theta,\alpha}$ =the gap fraction for the sun map sector;
$\cos(AngIn_{\theta,\alpha})$ = the angle of incidence between the centroid of the sky sector and the axis normal to the surface

In our research, we took into account the technical requirements for installing these panels. Depending on the geographical location, it is necessary to determine the appropriate tilt angle of the panels and their orientation relative to the south. The panels generate the most energy when the sun's rays strike the surface of the cells perpendicularly. To achieve high efficiency of an installed system in Poland, it should be oriented toward the south and set at an optimal tilt angle of 30° to 40°. Accordingly, the following factors were taken into account in the solar radiation calculations: roof tilt angles, roof slope exposure, the annual variation in the angle of incidence of sunlight, and atmospheric transmittance.

This contribution has been peer-reviewed.
https://doi.org/10.5194/isprs-archives-XLIX-B2-2026-1099-2026 |

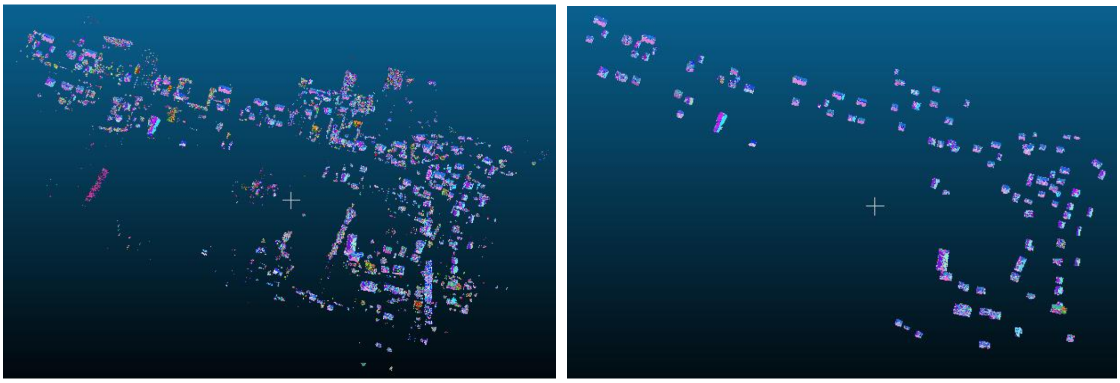

(a) (b)

Figure 5. Roofs detected using the (a) SVC and (b) SVC+ CANUPO algorithms

The roof pitch angles and exposure (which are essential for accurately determining the Sun's position relative to the roof surface) were determined from a digital roof model generated from a UAV point cloud. To develop the roof model, a DSM was generated from a point cloud containing only previously detected roofs. Points on the model that are not roofs are assigned a value of 0. The raster model was generated using Delaunay triangulation and linear interpolation, in accordance with equation (3)

$$DSM_{(i,j)} = \begin{cases} TIN\left(H_{P_{(i,j)}}, r\right), \text{if } P_{(i,j)} \in A \\ 0, if\ P_{(i,j)} \notin A \end{cases} \quad (3)$$

where $H_{P_{(i,j)}}$= the height of point *P* with coordinates *(i, j)* in point cloud *A*
TIN = triangle mesh interpolation algorithm (Delaunay triangulation)
r = spatial resolution of the elevation model (in our study, r = 1.0 m)

The angle of incidence of sunlight also depends on the date. In our study, we took into account the average angle of incidence of sunlight over the course of a year and on a quarterly basis (which is important given the changes in the angle of incidence of sunlight throughout the year). The result of this stage was a map identifying suitable locations for the installation of photovoltaic panels.

4. Results and discussion

In this article, we describe the application of the SVC+CANUPO algorithm for roof detection in the analysis of solar irradiance and the prediction of optimal locations for the installation of photovoltaic panels. Subsection 4.1 provides a detailed evaluation of the algorithm's effectiveness. In subsection 4.2, we present the results of the solar irradiance analysis.

4.1 The effectiveness of roof detection

In our experiment, we evaluated the effectiveness of the SVC+CANUPO algorithm for roof detection. Figure 5 shows the results of roof detection using SVC alone and SVC+CANUPO. Even a visual analysis reveals that CANUPO is significantly more effective. Using SVC alone allowed for the detection of roofs, but there were also many false positives, such as trees and building facades. The additional CANUPO classification made it possible to filter out non-roof objects and obtain a clean roof class.

We performed a quantitative evaluation of the resulting point clouds (after filtering). We calculated metric values commonly used to assess the quality of the detected class, such as Precision, Recall, F1-score, and Accuracy. Table 2 summarizes the results of the quality assessment of roof detection from the point cloud generated after multi-image matching from UAV data. The resulting model achieves 100% precision. No incorrect detections were found for the analyzed area. All detections corresponded to actual roofs. However, the proposed model did not detect all buildings. Most of the omissions were small roofs in green and greenish-gray. Consequently, Recall and Accuracy were 0.75, while the F1 score was 0.86. These values demonstrate the high effectiveness of the proposed approach in roof detection.

metric	value	equation
TP (true positive)	115	All correctly detected roofs
FP (false positive)	0	All false positives
FN (false negative)	38	Missing detections
Precision	1.0	$Precission\ = \frac{TP}{TP + FP}$
Recall	0.75	$Recall\ = \frac{TP}{TP\ +\ FN}$
F1-score	0.86	$F1 = 2 \cdot \frac{precision\ \cdot\ recall}{precision\ +\ recall)}$
Accuracy	0.75	$Accuracy = \frac{TP}{TP + FP + FN}$

Table 2. Quality metrics for roof point clouds after applying the SVC+CANUPO algorithm.

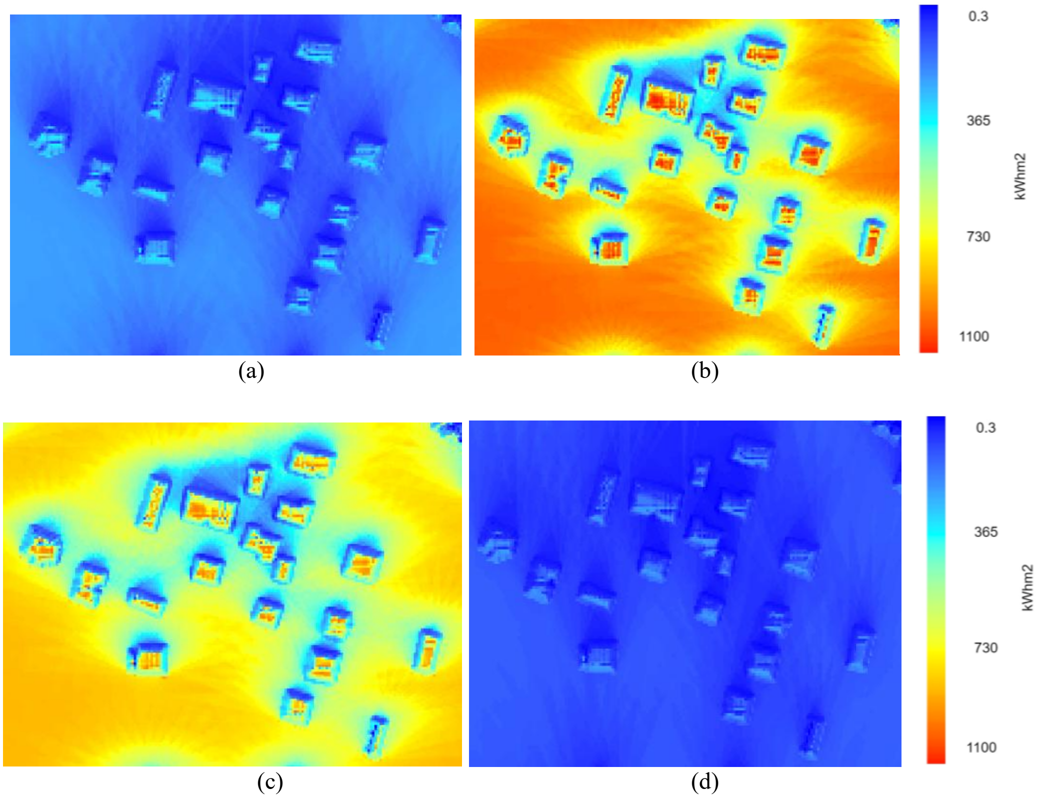

Figure 6. Analysis of solar insolation for (a) the first quarter (January 1–March 31); (b) the second quarter (April 1–June 30); (c) the third quarter (July 1–September 30); (d) the fourth quarter (October 1–December 31).

(Kushwaha et al., 2019) proposed a similar solution by combining the CSF Filter and the CANUPO Classifier to extract roof coverings and facades from a UAV point cloud for a densely built-up area. However, the goal of their research was to perform segmentation without conducting further analysis. In their work, they achieved an accuracy of approximately 85%, which demonstrates that the CANUPO model can also be highly effective in analyses of areas with high-density development.

4.2 Analysis of solar insolation

An analysis of the roofs surveyed clearly shows that the southern and central parts of the roof receive the most sunlight, which is due to Poland's location in the Earth's northern hemisphere. In areas located north of the Tropic of Cancer, the southern side will always be better illuminated. In contrast, the opposite is true in the Southern Hemisphere, where the Sun is highest in the north, so the northern side of roofs will be better illuminated. Figure 6 shows the results of roof detection using the CVC+CANUPO algorithm. Colors ranging from blue to red indicate the level of solar insolation on the roof, with red indicating the strongest insolation (over 1000 kWh/m²). The results show that the most sunlight reaches the central parts of the roofs on the south side. Overall, on the south side of the roof, it is possible to obtain over 730 kWh/m² per year.

The Earth's orbit around the Sun causes changes in the Earth's illumination, namely changes in the angle of incidence of sunlight, changes in the Sun's altitude, changes in the length of day and night, and the occurrence of seasons in the region of Poland (moderate latitudes). Therefore, in our study, we considered solar radiation for each quarter of the year.

The lowest solar insolation is observed in the fourth quarter, i.e., from October 1 to December 31 (Figure 6(d)). During this part of the year, the length of the day shortens and the Sun is low on the horizon, resulting in an energy yield of approximately 70 kWh/m². The situation is significantly better in the first quarter of the year (January–March, Figure 6(a)), when the length of the day increases. At that time, it is possible to obtain energy equal to approximately 150 kWh/m² on the southern and central parts of the roof. In the second (April–June, Figure 6(b)) and third (July–September, Figure 6(c)) quarters, solar insolation is highest, reaching up to 450 kWh/m².

In addition, the analyses took into account the relationship between different roof types and solar radiation, as in the study by (Martín-Jiménez et al., 2020). There were 153 buildings in the study area, with a total roof area of 16 110 m². Figure 7 shows the percentage share and area of individual roof types, taking into account their shape (flat, single-slope, gable, hipped, and multi-slope roofs) and slope angle (from 0° to 50°). The most common were gable roofs, which are popular in Poland and covered a total area of over 7 000 m² (accounting for 46% of the total roof area). Our research has confirmed that when installing photovoltaic panels on such roof surfaces, their exposure must be taken into account. When the roof has a north-south orientation, the panels should be installed on the south side, as close to the roof ridge as possible. In contrast, with an east-west orientation, cells placed on the west side of the roof will generate more energy.

For hip roofs and multi-pitched roofs, the best orientation is to have as much surface area as possible facing south and/or southwest. The closer to the roof ridge, the stronger the sunlight. Flat roofs, where sunlight is evenly distributed, were a distinct minority. In such cases, it is recommended to install panels on special structures facing south. There were no single-slope roofs in the study area. However, based on the conducted analyses, it can be concluded that installing panels on north-facing roofs

https://doi.org/10.5194/isprs-archives-XLIX-B2-2026-1099-2026

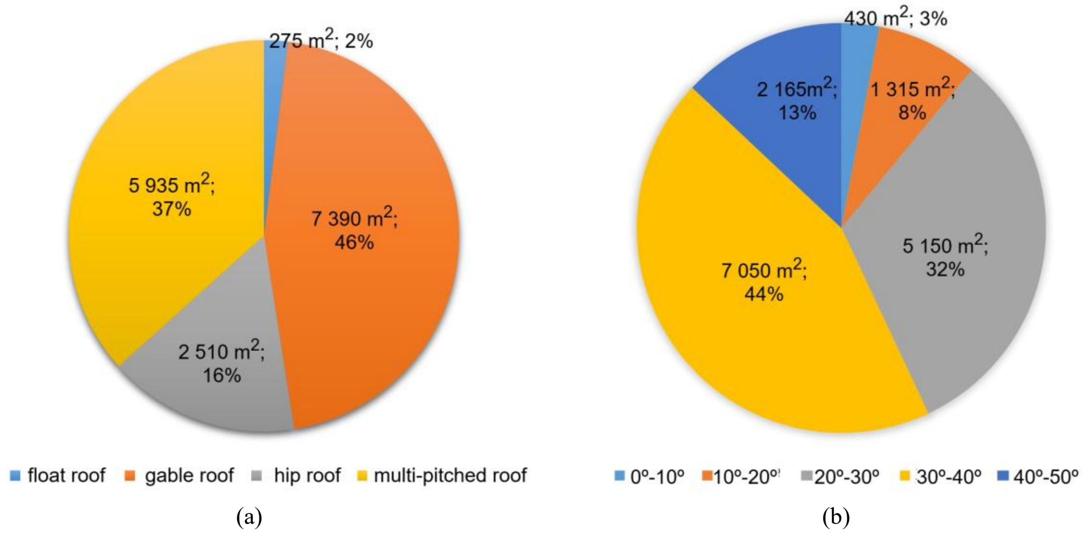

Figure 7 . A summary of roofs in the area of interest (a) by roof shape (b) by roof pitch.

would be uneconomical; in other directions, panels should be installed as close to the roof ridge as possible.

An analysis of roof slopes shows that the shallower the slope, the more even the sunlight radiation. At the same time, the highest parts of the roofs on the south side receive the most sunlight, making them the best locations for installing photovoltaic panels. The conducted sunlight insolation analyses can be compared to the results obtained by(Witkowska and Bielecka, 2014), The conducted sunlight insolation analyses can be compared to the results obtained by (Witkowska and Bielecka 2014), who in their study examined the use of LiDAR data to analyze roof slope and exposure for the installation of solar collectors. The study area consists of suburban areas. To calculate annual solar insolation, all elements (buildings, etc.) were taken into account. in our study, we considered only roof coverings, as the area under consideration is a rural area with low-density development. In both studies, the largest surface area consists of roof slopes inclined at angles ranging from 20º to 40º. Both our study and that of (Witkowska and Bielecka, 2014) showed that for most buildings, it is possible to effectively generate energy from photovoltaic cells installed on the roof surfaces. In other solar radiation analyses (Błaszczak-Bąk et al., 2025) however, the roof pitch and orientation were determined using a 3D building model

5. Conclusion

Our methodology enabled us to identify approximately 80% of the roofs on which locations for installing photovoltaic panels were subsequently designated. Our algorithm did not produce false positives in sparsely urbanized areas. The results confirmed that the southern and central parts of Poland's roofs receive the most sunlight. The opposite is true in the Southern Hemisphere, where the sun is highest in the north, so the northern side of roofs will be better illuminated. The lowest solar radiation in Poland is observed in the fourth quarter, i.e., from October 1 to December 31 (energy yield is then approximately 70 kWh/m²). In the first quarter of the year (January–March), the length of the day increases, and it is then possible to generate up to approximately 150 kWh/m² on the southern and central parts of the roof. In the second (April–June) and third (July–September) quarters, solar radiation is highest, reaching up to 450 kWh/m². The use of DSM for roofs and the SVC algorithm combined with CANUPO allowed for the elimination of false detections and a significant increase in the effectiveness of location detection. Studies conducted for the entire year and for individual quarters enabled an analysis of changes in roof insolation throughout the year, which is crucial when estimating the cost-effectiveness of installing photovoltaic panels.

References

Błaszczak-Bąk, W., Pacześniak, M., Oleksiak, A., Grunwald, G., 2025. UAV and 3D Modeling for Automated Rooftop Parameter Analysis and Photovoltaic Performance Estimation. Energies 18. https://doi.org/10.3390/en18205358

Bognár, Á., Loonen, R. c. g. m., Hensen, J. l. m., 2021. Calculating solar irradiance without shading geometry: a point cloud-based method. J. Build. Perform. Simul. 14, 480–502. https://doi.org/10.1080/19401493.2021.1971765

Cardoso, A., Jurado-Rodríguez, D., López, A., Ramos, M.I., Jurado, J.M., 2024. Automated detection and tracking of photovoltaic modules from 3D remote sensing data. Appl. Energy 367, 123242. https://doi.org/10.1016/j.apenergy.2024.123242

Cortes, C., Vapnik, V., 1995. Support-vector networks. Mach. Learn. 20, 273–297. https://doi.org/10.1007/BF00994018

Ekawita, R., Almadi, I.F., Yuliza, E., 2025. Investigating rooftop solar energy potential in coastal area with unmanned aerial vehicle technology. J. Energy Syst. 9, 1–11. https://doi.org/10.30521/jes.1416277

Guo, L., Deng, X., Liu, Y., He, H., Lin, H., Qiu, G., Yang, W., 2021. Extraction of Dense Urban Buildings From Photogrammetric and LiDAR Point Clouds. IEEE Access 9, 111823–111832. https://doi.org/10.1109/ACCESS.2021.3102632

He, M., Zhu, Q., Du, Z., Hu, H., Ding, Y., Chen, M., 2016. A 3D Shape Descriptor Based on Contour Clusters for Damaged Roof

Detection Using Airborne LiDAR Point Clouds. Remote Sens. 8. https://doi.org/10.3390/rs8030189

Henry, C., Poudel, S., Lee, S.-W., Jeong, H., 2020. Automatic Detection System of Deteriorated PV Modules Using Drone with Thermal Camera. Appl. Sci. 10, 3802. https://doi.org/10.3390/app10113802

How solar radiation is calculated—ArcGIS Pro | Documentation [WWW Document], n.d. URL https://pro.arcgis.com/en/pro-app/latest/tool-reference/spatial-analyst/how-solar-radiation-is-calculated.htm (accessed 3.27.26).

Huerta Herraiz, Á., Pliego Marugán, A., García Márquez, F.P., 2020. Photovoltaic plant condition monitoring using thermal images analysis by convolutional neural network-based structure. Renew. Energy 153, 334–348. https://doi.org/10.1016/j.renene.2020.01.148

Kaya, E., 2026. Assessment of building extraction and geometric corrections from UAV image using Mask R-CNN deep neural network algorithm. Eur. J. Remote Sens. 59, 2618374. https://doi.org/10.1080/22797254.2026.2618374

Kushwaha, S.K.P., Dayal, K.R., Singh, A., Jain, K., 2019. BUILDING FACADE AND ROOFTOP SEGMENTATION BY NORMAL ESTIMATION FROM UAV DERIVED RGB POINT CLOUD. Int. Arch. Photogramm. Remote Sens. Spat. Inf. Sci. XLII-2-W17, 173–177. https://doi.org/10.5194/isprs-archives-XLII-2-W17-173-2019

Ma, T., Zhu, H., Huang, W., An, P., Wang, C., Yu, K., 2023. Stereo Image Dense Matching Based on SGM Constrained by Feature Matching, in: 2023 9th International Conference on Computer and Communications (ICCC). Presented at the 2023 9th International Conference on Computer and Communications (ICCC), pp. 1911–1915. https://doi.org/10.1109/ICCC59590.2023.10507454

Martín-Jiménez, J., Del Pozo, S., Sánchez-Aparicio, M., Lagüela, S., 2020. Multi-scale roof characterization from LiDAR data and aerial orthoimagery: Automatic computation of building photovoltaic capacity. Autom. Constr. 109, 102965. https://doi.org/10.1016/j.autcon.2019.102965

Montesinos López, O.A., Montesinos López, A., Crossa, J., 2022. Support Vector Machines and Support Vector Regression, in: Montesinos López, O.A., Montesinos López, A., Crossa, José (Eds.), Multivariate Statistical Machine Learning Methods for Genomic Prediction. Springer International Publishing, Cham, pp. 337–378. https://doi.org/10.1007/978-3-030-89010-0_9

Nex, F., Remondino, F., 2012. AUTOMATIC ROOF OUTLINES RECONSTRUCTION FROM PHOTOGRAMMETRIC DSM. ISPRS Ann. Photogramm. Remote Sens. Spat. Inf. Sci. I–3, 257–262. https://doi.org/10.5194/isprsannals-I-3-257-2012

Ntuli, S.S., Akombelwa, M., Forbes, A., Singh, M., 2024. Classification of 3D Sonar Point Clouds derived Underwater using Machine and Deep Learning (CANUPO and RandLA-Net) Approaches. South Afr. J. Geomat. 13.

Shajahan, D.A., Nayel, V., Muthuganapathy, R., 2020. Roof Classification From 3-D LiDAR Point Clouds Using Multiview CNN With Self-Attention. IEEE Geosci. Remote Sens. Lett. 17, 1465–1469. https://doi.org/10.1109/LGRS.2019.2945886

Silva, A.S., Moraes Neto, F.H.A., Ferreira, P.H., Costa, D.B., 2025. CNN-Based YOLOv12 for Damage Assessment in Residential Roofs. IEEE Access 13, 193311–193322. https://doi.org/10.1109/ACCESS.2025.3629630

Singh, S.K., Raval, S., Banerjee, B., 2021. A robust approach to identify roof bolts in 3D point cloud data captured from a mobile laser scanner. Int. J. Min. Sci. Technol. 31, 303–312. https://doi.org/10.1016/j.ijmst.2021.01.001

Tarsha-Kurdi, F., Landes, T., Grussenmeyer, P., 2007. Hough-Transform and Extended RANSAC Algorithms for Automatic Detection of 3D Building Roof Planes from Lidar Data.

Witkowska, A., Bielecka, E., 2014. Analysis of exposure and slope of roofs for photovoltaics installation based on airborne scanning data 63 (2), 103–115.

Yang, J., Kang, Z., Akwensi, P.H., 2021. A Label-Constraint Building Roof Detection Method From Airborne LiDAR Point Clouds. IEEE Geosci. Remote Sens. Lett. 18, 1466–1470. https://doi.org/10.1109/LGRS.2020.2999818

Zhang, C., Fan, H., 2022. An Improved Multi-Task Pointwise Network for Segmentation of Building Roofs in Airborne Laser Scanning Point Clouds. Photogramm. Rec. 37, 260–284. https://doi.org/10.1111/phor.12420